

Observations of elemental carbon and absorption during ACE-Asia and implications for aerosol radiative properties and climate forcing

P. Y. Chuang,¹ R. M. Duvall,² M. S. Bae,² A. Jefferson,³ J. J. Schauer,² H. Yang,⁴
J. Z. Yu,⁴ and J. Kim⁵

Received 30 November 2002; revised 3 June 2003; accepted 10 June 2003; published 19 September 2003.

[1] Measurements of elemental carbon (EC) during the Asian Pacific Regional Aerosol Characterization Experiment (ACE-Asia) show that significant amounts of EC were found in the coarse particle phase during yellow sand events. Coagulation during long-range transport is consistent with this observation. The daily averaged specific mass absorption efficiencies of EC were calculated, yielding values of 12.6 ± 2.6 and 14.8 ± 2.3 m²/g for PM₁₀ (particulate matter <10 μm diameter) and PM₁, respectively. On a limited number of days, the absorption efficiency for the coarse particles only (PM₁₀ – PM₁) was determined to be 5.7 ± 1.6 m²/g during dust days and 2.0 ± 1.0 m²/g for nondust days. These measurements suggest that fine particulate EC was internally mixed and that the dust was possibly somewhat absorbing. Specific mass absorption efficiency was observed to be inversely related to EC mass concentration, a result that does not appear to reflect only air mass aging effects. We speculate that if this observation holds on a global scale, it would reduce the effectiveness of a strategy for mitigating climate change by reducing EC emissions. Model simulations of idealized nonspherical dust radiative properties predict that scattering is strongly (by nearly a factor of 3) dependent on geometry, while absorption is a very weak function of geometry. The net change in shortwave absorption by polluted dust layers due to coagulation of EC with dust is predicted by model calculations to range between –42% and +58%, depending on the assumption about the initial mixing state of the EC and the dust optical properties, with the observations supporting values in the range of –10 to –40%.

INDEX TERMS: 0305 Atmospheric Composition and Structure: Aerosols and particles (0345, 4801); 0345 Atmospheric Composition and Structure: Pollution—urban and regional (0305); 0365 Atmospheric Composition and Structure: Troposphere—composition and chemistry; 0360 Atmospheric Composition and Structure: Transmission and scattering of radiation; 1610 Global Change: Atmosphere (0315, 0325); *KEYWORDS:* elemental carbon, absorption, dust

Citation: Chuang, P. Y., R. M. Duvall, M. S. Bae, A. Jefferson, J. J. Schauer, H. Yang, J. Z. Yu, and J. Kim, Observations of elemental carbon and absorption during ACE-Asia and implications for aerosol radiative properties and climate forcing, *J. Geophys. Res.*, 108(D23), 8634, doi:10.1029/2002JD003254, 2003.

1. Introduction

[2] One of the important atmospheric phenomena resulting from the presence of elemental carbon (EC) in atmospheric aerosols is the absorption of light in visible wavelengths. This absorption and subsequent atmospheric heating has been estimated to lead to top of atmosphere radiative forcings in the range of 0 to +0.5 W m^{–2}

[Intergovernmental Panel on Climate Change (IPCC), 2001], although more recent estimates have an upper bound of +0.8 W m^{–2} [Chung and Seinfeld, 2002; Jacobson, 2002]. In addition to this direct radiative forcing, it has also been suggested that this atmospheric heating can reduce cloudiness under certain conditions [Ackerman *et al.*, 2000]. Accurately understanding shortwave absorption by EC is therefore an important component of predicting future climate. It has been estimated that sources in China account for roughly one-fourth of the global anthropogenic EC emissions [Cooke *et al.*, 1999], although recent estimates of the submicron EC emission inventory from China are uncertain by at least a factor of 4 [Streets *et al.*, 2001]. Therefore insight into the effects of EC in the plume downwind of east Asia represents a significant step toward understanding both the global budget of shortwave absorption as well as climate in the western Pacific region.

[3] The occurrence of episodic aeolian dust storms caused by entrainment of mineral aerosol from desert regions leads to a different uncertainty in global radiative forcing.

¹Department of Earth Sciences, University of California, Santa Cruz, Santa Cruz, California, USA.

²Environmental Chemistry and Technology Program, University of Wisconsin-Madison, Madison, Wisconsin, USA.

³Climate Monitoring and Diagnostics Laboratory, NOAA, Boulder, Colorado, USA.

⁴Department of Chemistry, Hong Kong University of Science and Technology, Hong Kong.

⁵Meteorological Research Institute, Korean Meteorological Administration, Seoul, Republic of Korea.

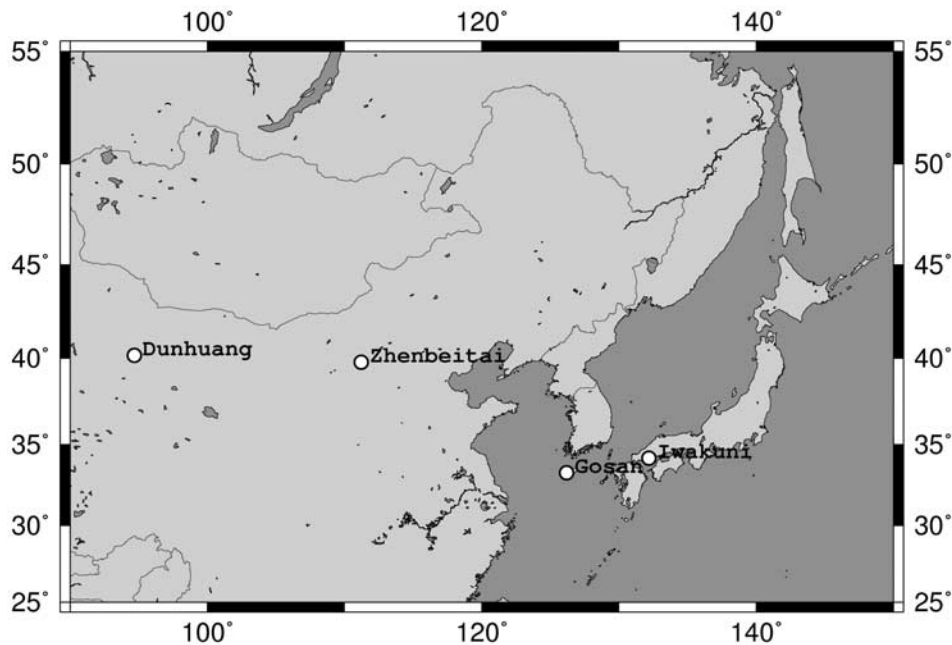


Figure 1. Map of the ACE-Asia region.

Because dust is generally a much weaker absorber of visible light than EC, the sign of the globally averaged net radiative forcing due to dust is as of yet unclear, with estimates in the range of -0.7 to $+0.5 \text{ W m}^{-2}$ [IPCC, 2001]. The major dust source regions of the world include the Sahara, northern and western China, and the Arabian Peninsula. In general, dust storms are not uniformly distributed in time, but rather concentrated during periods when weather patterns tend to bring conditions favorable for the lofting of dust to the free troposphere, such that these plumes can then be transported for long distances. In east Asia, the Kosa or yellow sand episodes are most common in late winter and spring, and on occasion their effects can extend as far as North America.

[4] One of the primary goals of the Asian Pacific Regional Aerosol Characterization Experiment (ACE-Asia) campaign (for an overview, see Huebert *et al.* [2003]) was to improve understanding of the physical, chemical, and radiative properties of the major east Asian aerosol types and the processes that control their evolution. Here, we report observations of EC during ACE-Asia at Gosan (Figure 1) and examine the implications for both aerosol optical properties and direct radiative climate forcing, with emphasis on periods during which high levels of EC were observed simultaneously with large amounts of mineral dust.

2. Observations of EC

2.1. Measurement Method

[5] Measurements were made at the Gosan (also referred to as Kosan), South Korea surface network supersite during the ACE-Asia campaign (Figure 1). The site is at the western tip of Jeju Island, about 50 m ASL. Winds from the westerly sector (NW to SW) are advected from China directly over the Yellow Sea or East China Sea, and sampled at Gosan with very little local influence (J. S. Park *et al.*,

Anthropogenic and desert-derived trace elements downwind of the Asian continent during the ACE-Asia experiment, submitted to *Journal of Geophysical Research*, 2003). These air masses therefore reflect aged continental air masses from east Asia. The wind direction is not always from this sector, however, and air masses that have most recently encountered land at Jeju Island, the Korean peninsula and Japan are also encountered. Two main periods of dust were encountered at Gosan during the intensive field sampling period: 1–13 April and 24–27 April (Julian Days 100 to 103 and 114 to 117, respectively). The first event exhibited substantially larger TSP (total suspended particulates) mass concentrations, with an average of $350 \mu\text{g/m}^3$, as compared to the second event, which had an average of $170 \mu\text{g/m}^3$. Both of these values are, as expected, much larger than the nondust event average mass TSP loading of $71 \mu\text{g/m}^3$.

[6] A large suite of TSP, PM_{2.5} (particulate matter <2.5 μm diameter), and PM₁ filters were acquired daily during the ACE-Asia campaign between 30 March and 2 May 2001. All filters were acquired at ambient temperature and RH. PM_{2.5} and PM₁ cutoffs were achieved using cyclone impactors. Using these substrates, a number of analyses can be performed, including: mass, EC, OC, major anions and cations, trace metals (including isotopes of Sr, Pb, Fe, and S), soluble OC, soluble metals, and organic speciation. The results of the EC measurements will be described here, while analyses of other measurements will be reported in future articles. Samples for EC analysis were collected on baked quartz fiber filters (Pall Life Sciences) and stored in a freezer in baked Al foil-lined petri dishes. EC was measured using thermal evolution and combustion with pyrolysis, as detailed by Schauer *et al.* [2003] for the TSP, PM_{2.5}, and PM₁ size fractions. Each day, the filters were changed starting at roughly 0 UTC (9 AM local time), with a sampling duration of between 20 and 22 hr for each day.

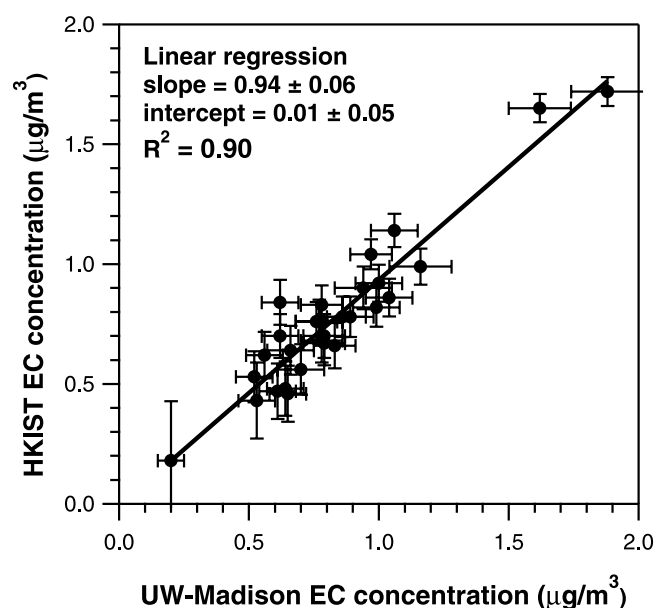


Figure 2. Comparison of independent EC mass concentration measurements for co-located samplers at Gosan.

[7] Along with EC concentrations, aerosol absorption coefficients b_{abs} were measured using a Particle Soot Absorption Photometer (PSAP, Radiance Research) at a wavelength of 565 nm and corrected to 550 nm. The uncertainty in b_{abs} is calculated on the basis of *Bond et al.* [1999]. The PSAP measurements were alternated between PM10 and PM1 in 6 min intervals.

2.2. EC Measurement Intercomparison

[8] One strong feature of the Gosan surface site was that a number of key measurements were made independently by different investigators, which strengthens confidence in the data when these independent measurements are in agreement. An intercomparison of the PM_{2.5} EC concentrations as measured by the University of Wisconsin-Madison and by the Hong Kong Institute of Science and Technology (HKUST) was performed (Figure 2). These are totally independent measures, as the filters were acquired and analyzed without consultation with the other group. The thermal desorption protocol used by both groups is identical. Figure 2 shows that this intercomparison is very good, with a slope of 0.94 ± 0.06 (all uncertainties herein are reported as 1σ), and an R^2 value of 0.90. This gives us confidence that the other University of Wisconsin-Madison EC measurements reported here are also accurate given the limitations of the protocol. HKUST did not measure EC for either PM1 or TSP, so it is not possible to make these comparisons.

2.3. Observations of Coarse Particle EC

[9] Figure 3 shows the daily concentrations of EC for the entire campaign period. One interesting observation is that during a number of those days strongly influenced by long-range dust transport, a significant fraction of EC is observed in the TSP size fraction that is not accounted for in the PM_{2.5} and PM1 samples. We will discuss this observation in greater detail below. For comparison, a typical urban EC concentra-

tion is roughly 1 to 5 $\mu\text{g}/\text{m}^3$, while rural continental values are lower, around 0.3 to 1 $\mu\text{g}/\text{m}^3$ [*Seinfeld and Pandis*, 1998].

[10] During six out of the eight yellow sand days sampled (all days except 10 and 11 April), the fraction of total EC that is measured to be in the coarse particle phase (greater than 1 μm aerodynamic diameter) is quite large. The average ratio of coarse mode EC to total EC for these six days is $39 \pm 11\%$ (1σ standard error). The $\pm 11\%$ standard error in the average ratio likely represents an upper bound in uncertainty, since recent work suggests that the uncertainty in EC concentration according to the thermal evolution standard operating procedure is overly conservative [*Schauer et al.*, 2003]. Therefore we believe that the observation of significant coarse mode EC is real and not an artifact of the measurement technique. This observation was initially unexpected, as EC is generally emitted into the atmosphere as particles with aerodynamic sizes smaller than 0.1 μm . In examining the literature, it was found that at least one previous study [*Parungo et al.*, 1994] observed the presence of soot on the surface of 40% of particles with diameter $> 2\ \mu\text{m}$, although they did not quantify the mass concentrations of EC in these cases.

[11] Figure 3 also shows that there are a number of days (e.g., Days 99, 107, 120, among others) when a significant fraction of EC was found in the coarse mode, despite a lack of evidence that these days were strongly influenced by yellow sand. Examination of these data shows that these days exhibit average or higher mass concentrations of TSP. We speculate that some or all of these events may be weak Kosa events, or events that have been mixed with other air masses. Isentropic back trajectories are inconclusive in helping us resolve this question because of their inherent uncertainties. The observation of coarse EC during nondust days is interesting, and worth further investigation, but because they are more complex than the dust events, we will not pursue this further, although we note that the model results presented here (section 4) would pertain to these events also if the coarse mode is predominantly mineral dust.

[12] A number of physical mechanisms could be responsible for the observed coarse mode EC. We hypothesize here that coagulation timescales are consistent with the timescales of transport from the EC source regions, and is the likely mechanism. First, we must establish that the EC is not present in the dust when initially lofted into the atmosphere. This issue can be addressed by examining the analyses of filters collected at Dunhuang, China during the ACE-Asia campaign. Dunhuang is located within one of the dust source regions (see Figure 1 for its location), as seen by the very high aerosol loadings (TSP $\sim 1000\ \mu\text{g}\ \text{m}^{-3}$) during yellow sand events. On days dominated by dust storms, the mass fraction of EC for particles between PM_{2.5} and PM₅ collected at Dunhuang was 0.01%. In contrast, the mass fraction of EC for particles collected at Gosan in the size range between TSP and PM1 during the 6 dust days ranged from 0.1 to 0.6%. Although the size ranges do not perfectly overlap, the large difference between these mass fractions is likely an accurate indicator of a significant increase in EC associated with the coarse particles at Gosan relative to Dunhuang. Of course, there is no guarantee that the dust measured at Dunhuang is representative of the dust that was measured at Gosan. Back trajectories suggest that during the dust storms, air parcels passed somewhat near Dunhuang

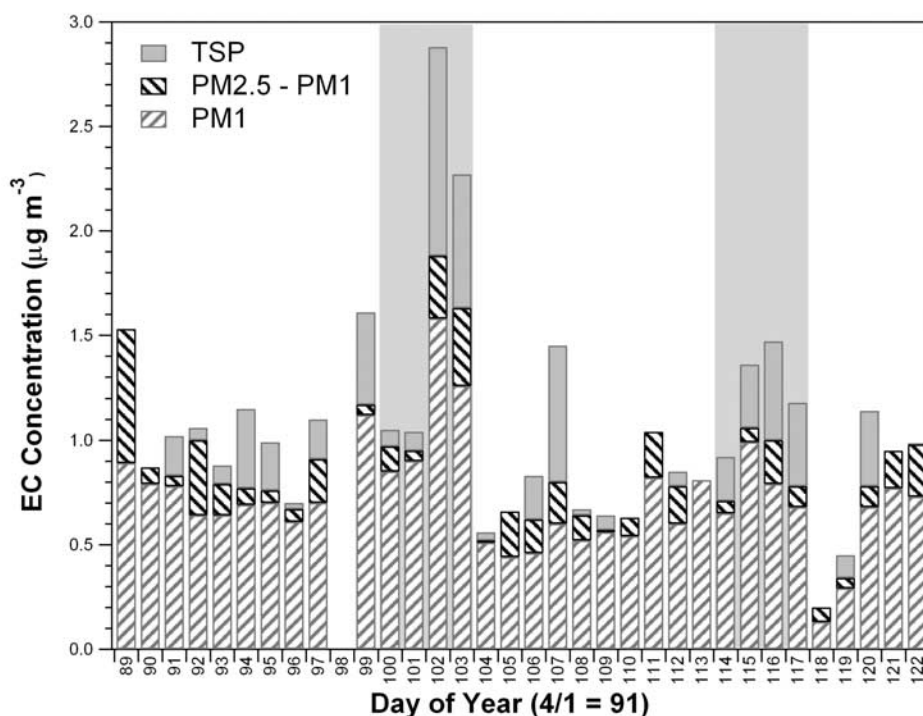


Figure 3. Daily Gosan mass concentrations of EC during the ACE-Asia intensive field campaign. Some data is missing because of problems with sample acquisition and handling or EC analysis. The shaded periods indicate the two Kosa episodes.

(within a few hundred kilometers) before reaching Gosan. This leads us to believe that EC is present on dust particles at greatly elevated concentrations at Gosan relative to the source dust regions.

[13] We examine next the timescale for coagulation necessary to lead to 40% of the EC mass to be associated with the coarse particle phase. The value of 40% was chosen because an average value of $39 \pm 11\%$ was found in the coarse particle phase during six of the dust event days. To simplify the analysis of the problem, we assume that the soot is initially found only in the fine particle phase, that the dust is only in the coarse particle phase, and that the distribution of each is monodisperse. Humidified tandem DMA (HTDMA) measurements aboard the CIRPAS Twin Otter during ACE-Asia show that it is most common for the smallest particles to be least hygroscopic (D. R. Collins, personal communication, 2002), which is consistent with the assumption that the soot is contained within the smallest particle sizes. The latter deduction seems reasonable because previous HTDMA measurements [McMurry *et al.*, 2002] have measured that those particles with the lowest hygroscopicity also exhibit the lowest density, consistent with a significant soot concentration in these particles. For soot sizes in the range between 20 and 60 nm diameter, and for the range of dust concentrations observed at Gosan with a mean diameter of 2 μm (estimated from measured size distributions), the time necessary for the partitioning of 40% of the soot to the dust is calculated to range between 20 and 80 hr. This timescale accounts for both Brownian and sedimentation coagulation, which are both important in the size ranges considered. This coagulation timescale agrees reasonably well with the estimated transport time-

scale of 60 hr (based on isentropic back trajectories) during which the dust and soot aerosol may be associated. This transport timescale is based on a map of EC emissions as a function of location [Streets *et al.*, 2001], which shows that EC is emitted in a large area that starts at the east coast and extends far inland, but not quite as far inland as many of the dust source regions. The point at which the back trajectories show that the air parcels first intersect the western edge of this EC source region, then, lies approximately 60 hr from Gosan. The likely physical picture, then, is one where the same meteorological conditions that lead to the lofting of dust into the free troposphere result in the same lofting of pollution aerosol downwind, and that the interaction of these two populations leads to substantial coagulation of fine mode pollution aerosol with coarse mode dust particles. Further coagulation of the dust aerosol after it re-enters into the boundary layer with boundary layer EC (perhaps more local or regional in nature) is also likely to contribute.

3. Observations of Specific Mass Absorption Efficiency α_a

[14] Because EC is the most important absorber of visible light, and east Asia is estimated to represent roughly one-quarter of the global EC budget [Cooke *et al.*, 1999], it is interesting to examine the efficiency with which the EC absorbs light. The specific mass absorption efficiency (hereafter also referred to in short as “absorption efficiency”) in units of m^2/g is defined for a single particle as:

$$\alpha_a = \frac{C_{abs}}{m_p} \quad (1)$$

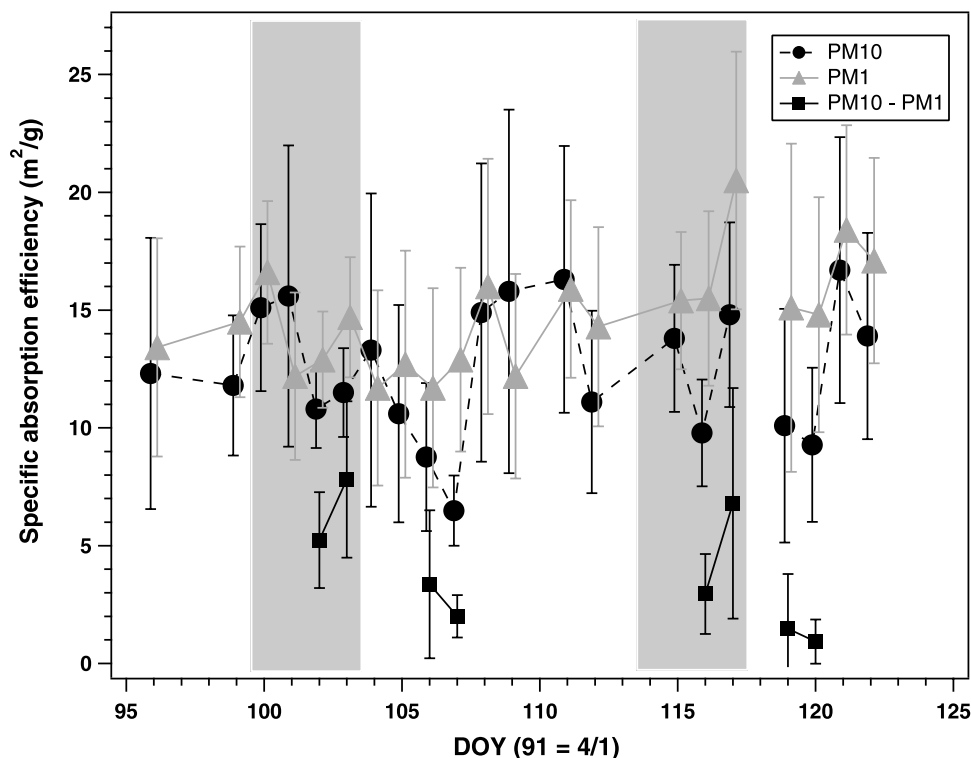


Figure 4. Daily specific mass absorption efficiencies for the PM10, PM1, and coarse (PM10 to PM1) particle fractions. Shaded areas represent the two yellow sand periods. Data are slightly offset from each other for clarity. Coarse particle fraction excludes error bars, which are generally quite substantial, about 50 to 120% of the derived efficiency value. See text for more discussion.

where C_{abs} and m_p are the absorption cross section (in m^2) and the particle mass (in grams). The absorption efficiency can also be defined for a population of particles as:

$$\alpha_a = \frac{b_{abs}}{M_{EC}} \quad (2)$$

where b_{abs} and M_{EC} are the absorption coefficient (in m^{-1}) and the mass concentration of EC (in $g\ m^{-3}$). See *Liou et al.* [1993] for a review of theoretical and experimental approaches for determining α_a . Model predictions for pure externally mixed EC particles show that α_a does not appear to exceed $10\ m^2/g$ at $\lambda = 550\ nm$, with a likely range of 4 to $8\ m^2/g$ for EC particles less than $0.2\ \mu m$ in diameter [Chylek, 1981; Fuller et al., 1999; Martins et al., 1998]. Measurements on commercially available soot are in agreement with these predictions [Clarke et al., 1987]. Variability of α_a is most likely governed by variability in aerosol mixing state, morphology, size distribution, and refractive index. Calculations of absorption efficiency for internal mixtures of soot with sulfate in the sub-micron size range show that in general the values are larger than for the external mixture case. Under very specific conditions of optical size and a soot inclusion location, values as large as $35\ m^2/g$ are possible; however, when the model predictions are averaged for randomly located inclusions and over a reasonable size distribution, the overall population absorption efficiency likely does not exceed $15\ m^2/g$ except under very clean conditions where the ratio of EC to sulfate is unrealistically low [Ackerman and Toon, 1981; Chylek, 1981; Fuller et al., 1999]. Previously observed values of α_a

for ambient aerosols, under conditions when internal mixtures are likely, support these larger values of α_a for a wide range of conditions [Liou et al., 1993, and references therein; Groblicki et al., 1981; Japar et al., 1986; Martins et al., 1998].

3.1. Method for Calculating α_a

[15] Figure 4 shows a timeline of the daily averaged absorption efficiency at Gosan for both PM10 and PM1. Shaded are the two major dust periods, 4/10 to 4/13 and 4/24 to 4/27. Figure 5 shows a histogram of these daily α_a values. The absorption efficiencies were calculated on the basis of equation (2). The error bars in Figure 4 reflect the propagated uncertainty in both EC concentration and b_{abs} . One sampling bias occurred because the filter cut-points were conducted with the sample at ambient RH, whereas the PSAP cut-points were conducted with the sample RH fixed at 50%. Ambient RH during the campaign ranged from 40 to 95% RH, with a median value of 71%. The variability that results from the diurnal cycle will not strongly affect these reported data because both the EC concentration and absorption measurements are integrated over one day. However, day-to-day variability will lead to biases. For ambient RH values above 50%, the cyclones upstream of the filter samples will remove more particles than those upstream of the PSAP, leading to α_a values that are biased high since EC mass will be biased low. This is difficult to correct for without detailed knowledge of the size distribution of EC in the vicinity of the PM1 cut point, and therefore we make no attempt here to adjust the data. We acknowledge that some amount of variability in α_a is

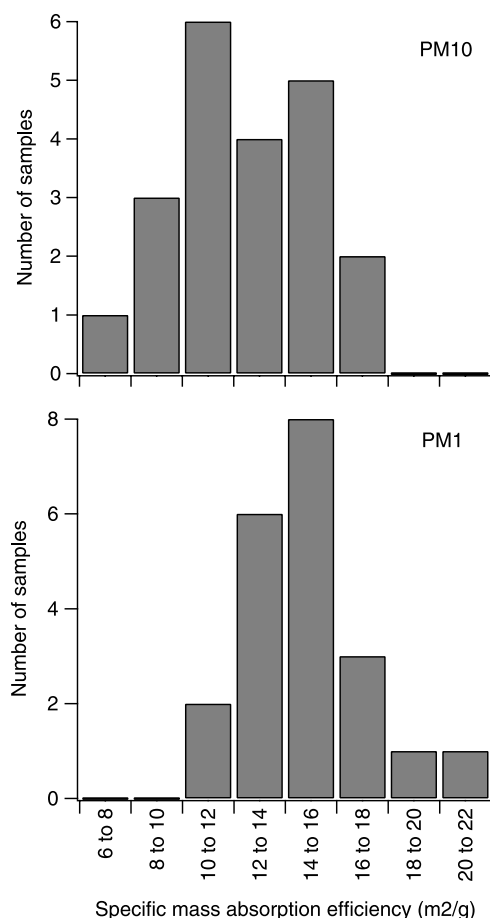


Figure 5. Histograms of daily averaged PM10 and PM1 specific mass absorption efficiencies.

therefore likely because of ambient RH differences, but given that the median RH was not much greater than the instrumental RH, it is likely that this bias does not strongly affect the results reported here. Another potential sampling bias occurs because the PSAP sampled PM10, while the comparable filter measurements were made without a cut-point, and therefore reflected TSP. This bias could lead to overestimates of PM10 EC mass, and therefore to underestimates of α_a . However, size distribution measurements at Gosan suggest that there did not exist significant surface area, which coagulation is sensitive to, above PM10, and therefore it appears unlikely that these very large particles would have served as a significant sink of fine-mode EC. Hereafter, we will refer only to PM10 rather than TSP measurements.

3.2. Observed PM1, PM10, and Coarse Mode α_a

[16] Figures 4 and 5 show that most of the measurements exceed the 4 to 8 m²/g efficiencies predicted for external mixtures. This suggests, then, that EC was predominantly internally mixed during the ACE-Asia intensive campaign. This observation is supported by the Twin Otter HTDMA ACE-Asia data, which shows that there was rarely a “low-hygroscopicity” mode at a growth factor (diameter ratio between RH < 20% and RH = 84%) in the range of 1.1 (D. R. Collins, personal communication, 2002) that is often characteristic of urban environments and has been attributed

to particles containing significant amounts of EC [McMurry *et al.*, 2002]. Figure 4 also shows that for the most part, there is a reasonable correlation between PM10 and PM1 absorption efficiency. The project mean and 1 σ variability of α_a in the PM10 and PM1 fractions are 12.6 ± 2.6 and 14.8 ± 2.3 m²/g. The correlation between the two size fractions is partly a function of the fact that PM10 includes the PM1 fraction, and therefore on those days when most of the EC is in the fine particle fraction, PM10 absorption efficiency will be nearly the same as that for PM1.

[17] For eight of the 22 days, including four of the eight dust days, the mass fraction of EC found in the coarse (PM10 minus PM1) size fraction was sufficient to allow for estimating α_a for just the coarse particulate matter. For the days when coarse α_a are not plotted, the estimated uncertainty far exceeded the calculated value (due to differencing of two terms in each the numerator and denominator), and these values have been omitted from Figure 4. For those data that were retained, the coarse particle mass absorption efficiency is substantially less than that for PM1. For the four dust days with reasonable uncertainties, coarse particulate α_a averaged 5.7 ± 1.6 m²/g, while the average was 2.0 ± 1.0 m²/g for the four nondust days shown, whereas 15.9 ± 1.8 m²/g and 13.6 ± 2.6 m²/g were observed for those same days, respectively, in the PM1 size fraction. The difference between dust and nondust days is consistent with the interpretation that yellow sand is much more strongly absorbing than normal coarse particulate matter. Because absorption efficiencies are normalized with respect to soot concentration, and if we assume that the soot that coagulates with dust exhibits a reasonably consistent absorption efficiency, then the difference in α_a could be explained by the presence of additional absorption by the dust itself. However, significant variability in soot characteristics such as primary particle size and morphology could also affect soot α_a and thereby also cause such a change in coarse particle α_a . More data would be needed to determine which of these possible explanations is more likely. One observation based on these eight days that might shed light on this issue is the suggestion of a correlation between coarse and fine particle α_a ; that is, these values fluctuate upward and downward synchronously for the most part. This observation may suggest that some of the variability in α_a is due to characteristics of the soot particle itself, independent of its coagulation with coarse mode particles, but again quantitatively evaluating this effect is not realistic with the limited data available.

3.3. Mass Fraction Dependency of α_a

[18] Figure 6 shows the absorption efficiency data plotted against the mass fraction of EC in the PM1 and PM10 size fractions. Models as well as laboratory studies have predicted that there is an inverse relationship between these two quantities for internal mixtures [Petzold *et al.*, 1997]; that is, as EC becomes more dilute, its absorption efficiency increases. While not a perfect correlation, this general trend is certainly observed for PM10, and seems to be present for PM1 also. Since α_a depends on a number of parameters as discussed above, it is unreasonable to expect EC mass fraction to explain perfectly the observed variability, but it does appear that it does play a role as theoretically predicted. One possible interpretation is that as EC mass

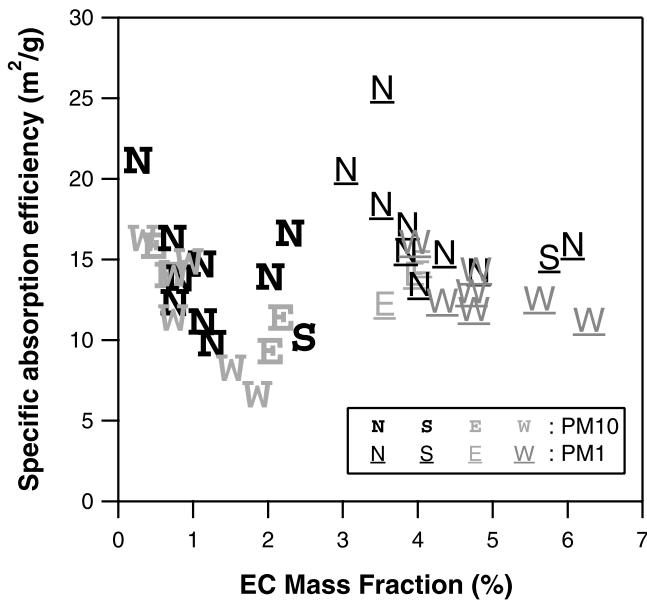


Figure 6. Specific mass absorption efficiency plotted as a function of EC mass fraction for the PM10 and PM1 fractions. The symbols represent wind directions from those sectors. N includes the N and NE directions; W includes NW, W, and SW; E includes E and SE. Only one day was classified as southerly wind direction. Underlined letters (N, E, S, W) are for PM1; the letters that are not underlined are for PM10.

fraction increases, a smaller fraction of the EC can effectively absorb light because of a shielding-type effect, although there may exist other possibilities also.

[19] One possible explanation for this observation could be that the degree of internal mixing increases with time, and therefore all dependency in Figure 6 is the result of air mass age. To test this, the data were segregated on the basis of wind direction. Winds from the W sector reflect the longest transport time because these aerosols come from continental Asia. Winds from the N sector also are impacted by the continent, although this last contact with land may have occurred in northern China or somewhere on the Korean peninsula, and therefore on average is probably less aged compared to W winds. Easterly winds are generally advected directly over Jeju island before reaching the sampling site, and therefore are most likely the least aged air masses. There was only one day with significant southerly flow. The results of segregating the data (Figure 6) show that there is no observed bias where E, W, and N trajectories exhibit increasing values of α_a due to increased air mass aging. We therefore believe that air mass aging is not the primary controlling factor for the observations in Figure 6.

[20] If this is a consistent feature of absorption by ambient aerosols, then it could be important for understanding the future impact of light absorption on climate as EC emissions change. It has been suggested [Hansen *et al.*, 2000; Jacobson, 2002] that control of EC emissions may be an effective strategy for mitigation of climate change. The possible concomitant increase in the average EC specific mass absorption efficiency would lead to a net benefit smaller than that assuming a linear response of absorption with changing EC mass concentration. In fact, the data in

Figure 6 suggests that it is plausible that a decrease of 50% in the EC concentration, with everything else held constant, could increase α_a by roughly a factor of 2, which would completely negate the intended decrease in shortwave absorption, although such quantification of this effect is premature and intended only to stimulate discussion. We stress that this is a preliminary result that is based on observations over a short period of time in one location, and therefore not necessarily applicable on a global scale, although Gosan is a location that is influenced by a number of different air mass types and therefore is a good regional-scale receptor site in an area with a significant fraction of the global EC output. These observations suggest that the issue of controlling EC for the purposes of mitigating global warming requires more research.

4. Model Predictions of Composite Soot and Dust Aerosol

[21] We seek to more carefully explore the implications of the coagulation of EC onto dust particles on shortwave absorption. Our observations are limited by large uncertainties (Figure 4), which leads us to turn to model simulations. We stress that our main intention is to address relative changes in absorption and scattering caused by the coagulation of dust and soot, rather than absolute numbers of, for example, dust single-scattering albedo, which is the subject of much current research [e.g., Kaufman *et al.*, 2001].

4.1. DDA Model Calculations

[22] Mie theory is often used to calculate scattering and absorption by atmospheric aerosols. It is, however, generally applicable to spherical, homogeneous particles, although extensions of Mie theory exist for other idealized particles such as those composed of spherically symmetric shells. Dust particles, on the other hand, are known to be very different from spheres. Electron micrograph images of dust particles from various regions of the world, including dust from China, show this clearly. Gao and Anderson [2001] analyzed such images for a parameter they termed “circularity” which is the ratio of the square of the perimeter to 4π times the two-dimensional area of the image. Using this measure, a spherical particle would have a circularity of 1.0, with other shapes exhibiting higher circularities (e.g., a square has a circularity of 1.27). For a location in China dominated by aeolian dust (Mt. Wali-guan), almost all particles were found to exhibit circularities larger than 1. The distribution is broad, with a mean circularity of about 2. To further complicate matters, soot has a refractive index very different from that of common minerals, and therefore this heterogeneity in optical properties further rules out the use of Mie theory calculations for our purposes here.

[23] The discrete dipole approximation (DDA) technique was used for simulating the radiative properties of dust and soot aerosols [Draine and Flatau, 1994; Purcell and Pennypacker, 1973], using the publicly available software DDSCAT (B. T. Draine and P. J. Flatau, User guide for the Discrete Dipole Approximation Code DDSCAT (Version 5a10), unpublished manuscript, 2000) (available at <http://arxiv.org/abs/astro-ph/0008151v4>). Briefly, this model approximates the particle as an array of discrete polarizable

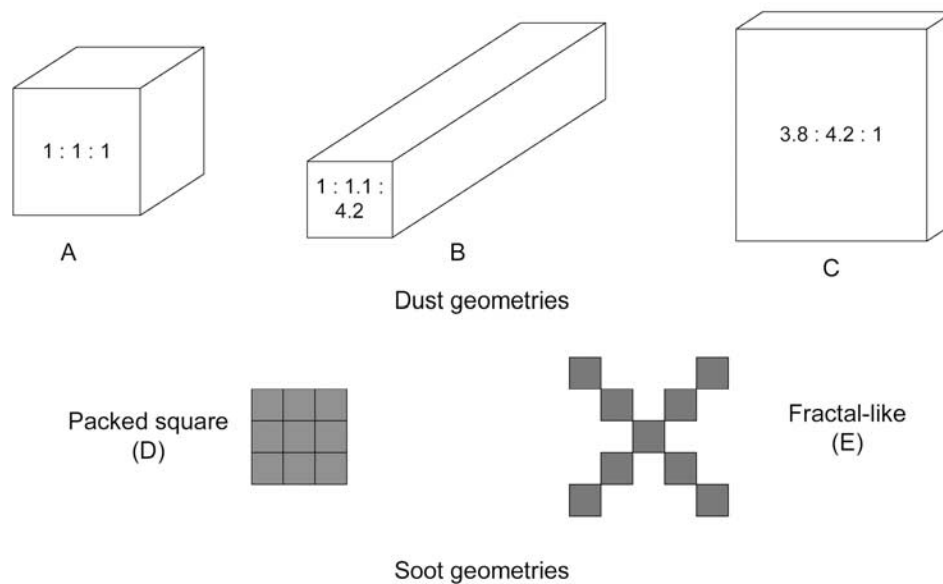


Figure 7. Simulated dust and soot geometries used for DDSCAT modeling of scattering and absorption. Note that the scale is different for the two aerosol types. The dust geometries are composed of 27,000 dipoles, whereas the soot is made of 9 dipoles as shown.

points on a cubic lattice. Scattering and absorption cross-sections from nonspherical particles and particles with nonhomogeneous compositions are then calculated (see B. T. Draine and P. J. Flatau (unpublished manuscript, 2000) for more details).

[24] Using this model, the absorption and scattering for a population consisting of a number of soot particles and one dust particle, all separate (i.e., an external mixture), is calculated and compared with the case where all the particles in the above population have coagulated such that all the soot particles are deposited on the surface of the dust particles. The dust particles are modeled using three idealized shapes (as shown in Figure 7): a cube (geometry A); a nearly square rod (geometry B); and a flat square (geometry C). Such regular shapes do not exactly model real dust particles, but in examining images of dust particles from the east Asian region, they do seem to reasonably span the range of particle shapes. For the purposes of coagulation with the dust, soot was modeled using two idealized geometries (Figure 7), one a packed matrix, and a second an X-shaped particle, which is intended to be a more physically realistic picture of what a soot agglomerate might look like in the atmosphere, with a larger fractal dimension than the packed matrix.

[25] The light scattering and absorption were modeled to examine the difference between (a) an external mixture of multiple soot particles and a single dust particle, and (b) a particle where the soot particles are all attached to the surface of the dust particle. First, the light scattering from the dust along for geometries A, B, and C were calculated. For all cases, the dust had an effective diameter (defined as the diameter of the equivalent-volume sphere) of $1.12 \mu\text{m}$, and the wavelength of light was 550 nm . The grid spacing was $0.03 \mu\text{m}$, and therefore each dust particle was composed of 27,000 dipoles. Each soot particle was represented as 9 dipoles, leading to an effective particle diameter of $0.078 \mu\text{m}$. The $0.03 \mu\text{m}$ dipole spacing leads to a primary

soot particle diameter in geometry E of $0.037 \mu\text{m}$, a reasonable value. To calculate C_{ext} and C_{abs} for each modeled particle, between 300 and 1000 orientations of the particle with respect to the incident radiation are averaged. Performing such orientation averaging is important for understanding the average optical behavior of particles in the atmosphere. Two values of the refractive index $m = n + ik$ were used (a) one representative of a mineral which is somewhat absorbing (e.g., hematite), $m = 1.6 + 0.007i$, and (b) a mineral with the same real refractive index but exhibiting almost no absorption, $m = 1.6 + 10^{-5}i$. The observations suggest that the dust observed at Gosan was slightly absorbing (section 3.2), although not very conclusively. We believe that these two cases represent bounding values of refractive index, and that the observed cases lie somewhere in between. EC was assigned a refractive index of $m = 1.96 + 0.66i$. All refractive indices are from *Seinfeld and Pandis* [1998]. Using these parameters, the scattering and absorption cross sections C_{scat} and C_{abs} were modeled, from which the specific mass absorption efficiency can be calculated using equation (1).

[26] To establish the optical properties of externally mixed dust and soot, C_{scat} and C_{abs} were modeled for both pure dust particles and pure soot aerosol. To verify the low-resolution soot-only calculations, additional runs were performed for geometries where the soot particle is represented as a single sphere (550 dipoles), and one where it is a chain of three spheres joined in a straight line (4224 dipoles). A comparison of the scattering and absorption cross sections for all of the soot geometries are in very reasonable agreement, implying that the results are not very sensitive to the choice of geometry, nor the number of dipoles used. Next, 22 soot particles were randomly deposited on the surface of each dust geometry. This was the number necessary to lead to a EC mass fraction of 0.4%, as derived from the coarse particle phase measurements at Gosan during the Kosa episodes. Soot geometry D was used for

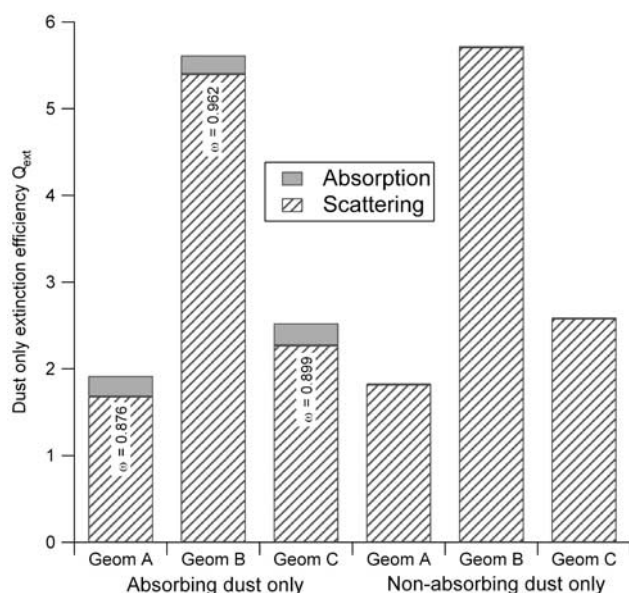


Figure 8. Model calculations of extinction efficiency Q_{ext} for the three dust geometries, with contributions of scattering and absorption separated, for two different refractive indices. Also shown are the single-scattering albedo ω in the absorbing dust case. The nonabsorbing dust has a single-scattering albedo of nearly unity. Note that in this plot, and also in Figure 9, the traditional extinction efficiency Q_{ext} (broken down into the components Q_{scat} and Q_{abs}) are plotted, rather than efficiencies normalized with respect to mass.

all three dust geometries, and soot geometry E was used with dust A to determine whether or not the results are sensitive to the soot geometry.

4.2. DDA Model Results

[27] Figure 8 shows the results for the dust particles only (no soot added) for both the absorbing and nonabsorbing dust cases. The differences in scattering and absorption are strictly a result of the different dust geometries A, B, and C that were used. The model calculations predict that large differences in scattering (greater than a factor of 3 between geometries A and B), can result simply from changing the dust geometry. These results qualitatively agree with one recent study that found significant differences in extinction coefficient as a function dust geometry [Kalashnikova and Sokolik, 2002]. Note, however, that the amount of absorption that occurs is a much weaker function of geometry for the absorbing dust (at most a 20% difference among the three geometries). This leads to a wide range in dust-only single-scattering albedo ω (where $\omega = C_{scat}/C_{ext}$) between 0.876 and 0.962, as seen in Figure 8. For the nonabsorbing dust, the model predictions show a very similar pattern in scattering efficiencies, but of course the single-scattering albedo remains nearly unity (not shown) because of the very small value of k .

[28] When soot is added to the dust particles, the model calculations yield results shown in Figure 9. Relative to pure dust, absorption increases by adding soot, as expected. At the same time, dust particle extinction changes very

slightly because of the addition of the soot particles. For geometry A, extinction actually decreases by about 2%, a result of scattering decreasing by an amount slightly greater than the increase in absorption. For geometries B and C, extinction increases and decreases, respectively, but by less than 0.5%. The values of ω therefore decrease (because the change in absorption is the strongest effect) as shown in Figure 9. For the absorbing dust case, the new range of ω is 0.846 to 0.948, a decrease of between 2 and 3%, while the nonabsorbing dust shows a decrease in ω from unity to between 0.961 and 0.985. These predictions of single-scattering albedo could be important for understanding the optical properties of aeolian dust in this region, which may have important implications for remote sensing measurements in addition to radiative forcing.

[29] For the purposes of understanding the radiative forcing by aerosols, the overall population single-scattering albedo (as opposed to that for only the dust particles) is the relevant parameter. By assuming that the EC particles were purely composed of EC and therefore externally mixed prior to coagulation, the amount of absorption for the entire population can be predicted, and then compared to that for the case where all these particles are coagulated into one larger particle; that is, we compare the absorption cross section due to unpolluted dust separate from 22 soot particles (our base case), with that when dust and 22 soot particles are coagulated together as one composite particle. The change in absorption is shown in Table 1 for the nonabsorbing dust geometries. The results show that coagulation leads to an enhancement in the absorption cross-section, and therefore in the total amount of absorbed energy by a factor of between 18% and 58%. Extinction again remains very nearly constant, in all cases changing by less than 2%. This translates directly into a 18 to 58% increase in the specific mass absorption efficiency. The net effect of coagulating externally mixed EC with nonabsorbing dust, therefore, is an

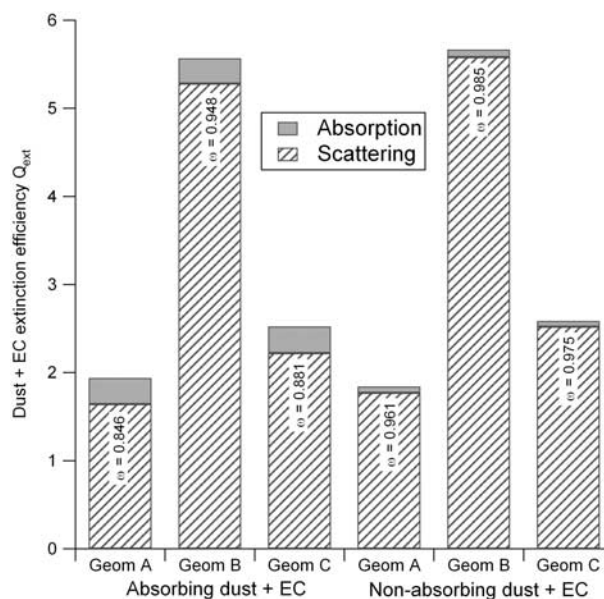


Figure 9. Same as Figure 8, except that EC has been added to the surface of the dust in proportion to that observed (Figure 3) during the dust events.

Table 1. Model Predictions of the Change in Total Shortwave Absorption as a Function of Initial Soot Mixing State, Dust Refractive Index, and Dust Geometry^a

Calculation Parameters		Change in Total Absorption Due to Coagulation		
Soot Initial Mixing State	Dust Refractive Index	Dust A/Soot D Geometry	Dust B/Soot D Geometry	Dust C/Soot D Geometry
External	absorbing	+2%	+8%	-2%
External	nonabsorbing	+31%	+58%	+18%
Internal	absorbing	-14%	-10%	-17%
Internal	nonabsorbing	-35%	-23%	-42%

^aSee Figure 7 for simulated dust and soot geometries. Selecting soot geometry E rather than D led to almost no change, and therefore the results are not shown here.

increase in absorption (and therefore in α_a), a slight decrease in scattering, and leading to a small net decrease in extinction, which leads to a net positive radiative forcing both at the top of atmosphere, and at the Earth's surface. For the absorbing dust cases, however, the results (Table 1) are somewhat different. Very little change in absorption occurs, as the absorption cross section of the soot is much smaller than that for the dust itself, and therefore very little net change occurs due to the coagulation of soot and dust.

[30] To show that these results are not specific to the size of dust particle chosen, a number of model runs were made with different sizes of nonabsorbing dust using geometry A. Table 2 shows the enhancement in absorption as a function of size. While not constant, this enhancement lies between +15% and +37% across the size range considered, which therefore shows that the results are not peculiar to the dust particle size chosen.

[31] Because these enhancement factors assume that the soot is initially externally mixed, the results likely represent the upper bound in the change in absorption due to coagulation. If the soot was initially internally mixed, the initial specific mass absorption efficiency would have been greater as discussed above, and coagulation would therefore lead to a smaller change in absorption enhancement, and possibly even to a decrease in overall energy absorption. To examine this question, the absorption efficiency of soot was increased by a factor of 2 to reflect EC that is initially internally mixed after which the model calculations were re-analyzed. This doubling in absorption efficiency was estimated on the basis of the fact that externally mixed soot has been predicted to have values of α_a in the range between 4 and 8 m²/g, whereas the PM1 values observed here (Figure 5) are somewhat greater, mostly in the range between 10 and 16 m²/g. By increasing α_a for soot aerosol only, then, the model calculations show a different story (Table 1). For the absorbing dust, coagulation leads to a change in overall aerosol absorption by -10 to -17% whereas before almost no change was seen. For nonabsorbing dust, coagulation is predicted to cause an even larger change in absorption, between -23 and -42%, whereas previously absorption was predicted to change by +18 to +58%. This comparison is not perfect because the model calculations for composite soot plus dust particles were not re-done to reflect additional nonabsorptive material internally mixed with EC. However, this is not expected to lead to large changes because scattering will be dominated by the dust particles in the composite particle. Therefore the model predicted net radi-

ative effects of EC coagulating with Asian dust is inconclusive in sign, as it depends strongly on the initial radiative properties of the individual soot-containing particles.

4.3. Comparison With Observations

[32] To compare these model results with observations, we again examine those four dust days when coarse and fine α_a were calculated with reasonable uncertainty (Figure 4). One net effect of the coagulation of soot with dust is a shift of soot from the PM1 fraction, where it has a generally high absorption efficiency, to the coarse particle fraction, where α_a is substantially lower. This in turn leads to a decrease in overall shortwave absorption in polluted east Asian dust plumes. Preliminary estimates show that if instead of 39% of the EC mass being in the coarse particle phase as was found during dust events, we assumed that this value was 27% (which is the average for all of the nondust days), then it is estimated that the observed average change in overall aerosol shortwave absorption due to coagulation would be -12% (averaged over the four days with good data). If we assume that 0% of the EC was in the coarse particle phase before coagulation (a comparison more in line with the setup of the model calculations), then the observed decrease in aerosol absorption would be -40%. Our previous model calculations predicted changes in range of -10 to -17% for internally mixed absorbing dust, and -23 to -42% for internally mixed nonabsorbing dust. Given the assumptions used in the calculations and the uncertainties in the observations, one probably should not draw any conclusions about the extent to which the mineral dust was absorbing. However, the fact that both observations and model predictions are consistent in showing similar reductions in absorption due to coagulation strengthens the case for this effect, and we therefore estimate the impact to be -10 to -40%, with values closer to -10% being more likely.

5. Other Effects

[33] Along with their radiative impacts, it is possible that the association of EC on dust particles during yellow sand events may have other important climate implications in the western Pacific region. If dry deposition is a significant removal mechanism for dust aerosols in this region, then the lifetime of EC in yellow sand episodes may be substantially decreased because of their association with dust particles, since the sedimentation velocities of the latter are much higher. If, on the other hand, wet deposition is the dominant removal mechanism, then there might be a much weaker

Table 2. Model Predictions of the Change in Mass Specific Absorption Efficiency of EC Due to Coagulation as a Function of Initial Dust Size, Assuming That EC is Initially Externally Mixed and the Dust is Nonabsorbing^a

Particle Diameter, μm	Change
0.4	+26%
0.5	+21%
0.6	+15%
0.8	+37%
1.1	+30%

^aThe soot mass fraction is constant (0.4%). There is no consistent trend with size, and the values are fairly consistent. We conclude that the model results are not specific to the size of dust particle chosen.

change in EC lifetime since collision efficiencies may decrease because of a smaller difference in sedimentation velocity between dust and collector precipitation drops.

[34] The deposition of Asian dust to the surface ocean is an important source of trace nutrients for marine biota in many regions of Pacific [Duce and Tindale, 1991]. The northern and equatorial Pacific regions are generally characterized to be HNLC (high-nutrient, low-chlorophyll) areas, where the primary nutrients N and P are not depleted, and it has been hypothesized that trace nutrient levels, particularly that of iron, limit growth in these regions [Martin and Fitzwater, 1988]. Therefore these regions may be particularly sensitive to changes in atmospheric trace metal fluxes to the ocean, as has been demonstrated in small-scale field experiments into iron fertilization [Coale et al., 1996]. We speculate here that simultaneous deposition of pollution aerosol with aeolian dust could affect ecosystems in a number of ways. The fraction of iron and other trace elements in mineral dust that is bioavailable is generally very low. It is possible that acids or other compounds present in the polluted particles could increase the amount of labile trace metals, thereby increasing biological productivity. On the other hand, organic compounds and other heavy metals are known to be biological toxins. The deposition of such compounds into the surface ocean could have a negative effect on ecosystem health, and the related issue of carbon deposition to the deep ocean. These issues are raised here as potentially very important but outside the realm of this study.

6. Summary

[35] The measurement of a significant fraction of EC (~40%) in the coarse particle phase during yellow sand events was not an a priori expected observation during the ACE-Asia campaign. We argue here that the combination of Brownian and sedimentation coagulation of fine aerosol with the coarse dust is a sufficient mechanism for this observation. Measured values of the specific mass absorption efficiency are 12.6 ± 2.6 and 14.8 ± 2.3 m²/g for the PM₁₀ and PM₁ fractions, respectively, in line with other reported measurements. For the four dust days and four nondust days for which statistically significant results were obtained, the coarse fraction only (PM₁₀ to PM₁) absorption efficiencies were 5.7 ± 1.6 m²/g and 2.0 ± 1.0 m²/g, respectively. The data suggest that the dust measured at Gosan, Korea, may have been absorbing, although these differences could also reflect differences in soot properties due to differing air masses. Observational evidence that EC increases in absorption efficiency as EC mass fraction decreases is presented, a preliminary result that could have important implications for atmospheric absorption and therefore climate, under a scenario where EC emissions are reduced. More research is needed to clarify this issue. Model calculations of dust using the discrete dipole approximation method show a strong (nearly a factor of 3) dependence of light scattering on dust geometry, but only a very weak dependence for absorption. The coagulation of dust and soot can significantly impact the total shortwave absorption by the aerosol population, and therefore the overall single-scattering albedo, but the sign of this change is unclear, depending strongly on the initial mixing state of

the particulate EC. Examining the model results and observations together suggests that the coagulation of EC onto the surface of dust particles during ACE-Asia significantly reduced overall shortwave absorption in these polluted dust plumes by values estimated to be on the order of -10 to -40%, with values closer to -10% being more likely.

[36] **Acknowledgments.** This research is a contribution to the International Global Atmospheric Chemistry (IGAC) Core Project of the International Geosphere Biosphere Program (IGBP) and is part of the IGAC Aerosol Characterization Experiments (ACE). Primary funding for this work has been provided by National Science Foundation grant ATM-0080814. Additional funding has been provided by the National Oceanic and Atmospheric Administration Office of Global Programs, the Research Grants Council of Hong Kong, and the Korea Ministry of Science and Technology through the National Research Laboratory Project. Helpful discussions with P. Flateau are also acknowledged.

References

- Ackerman, A. S., O. B. Toon, D. E. Stevens, A. J. Heymsfield, V. Ramanathan, and E. J. Welton, Reduction of tropical cloudiness by soot, *Science*, 288(5468), 1042–1047, 2000.
- Ackerman, T. P., and O. B. Toon, Absorption of visible radiation in atmosphere containing mixtures of absorbing and nonabsorbing particles, *Appl. Opt.*, 20(20), 3661–3668, 1981.
- Bond, T. C., T. L. Anderson, and D. Campbell, Calibration and intercomparison of filter-based measurements of visible light absorption by aerosols, *Aerosol Sci. Technol.*, 30(6), 582–600, 1999.
- Chung, S. H., and J. H. Seinfeld, Global distribution and climate forcing of carbonaceous aerosols, *J. Geophys. Res.*, 107(D19), 4407, doi:10.1029/2001JD001397, 2002.
- Chylek, P., Optical properties and mass concentration of carbonaceous smokes, *Appl. Opt.*, 20, 2980–2984, 1981.
- Clarke, A. D., K. J. Noone, J. Heintzenberg, S. G. Warren, and D. S. Covert, Aerosol light absorption measurement techniques: Analysis and intercomparisons, *Atmos. Environ.*, 21, 1455–1465, 1987.
- Coale, K. H., et al., A massive phytoplankton bloom induced by an ecosystem-scale iron fertilization experiment in the equatorial Pacific Ocean, *Nature*, 383(6600), 495–501, 1996.
- Cooke, W. F., C. Liou, H. Cachier, and J. Feichter, Construction of a 1° × 1° fossil fuel emission data set for carbonaceous aerosol and implementation and radiative impact in the ECHAM4 model, *J. Geophys. Res.*, 104(D18), 22,137–22,162, 1999.
- Draine, B. T., and P. J. Flatau, Discrete-dipole approximation for scattering calculations, *J. Opt. Soc. Am.*, 11(4), 1491–1499, 1994.
- Duce, R. A., and N. W. Tindale, Atmospheric transport of iron and its deposition in the ocean, *Limnol. Oceanogr.*, 36(8), 1715–1726, 1991.
- Fuller, K. A., W. C. Malm, and S. M. Kreidenweis, Effects of mixing on extinction by carbonaceous particles, *J. Geophys. Res.*, 104(D13), 15,941–15,954, 1999.
- Gao, Y., and J. R. Anderson, Characteristics of Chinese aerosols determined by individual-particle analysis, *J. Geophys. Res.*, 106(D16), 18,037–18,045, 2001.
- Groblicki, P. J., G. T. Wolff, and R. J. Countess, Visibility reducing species in the Denver “brown cloud”: I. Relationships between extinction and chemical composition, *Atmos. Environ.*, 15, 2473–2484, 1981.
- Hansen, J., M. Sato, R. Ruedy, A. Lacis, and V. Oinas, Global warming in the twenty-first century: An alternative scenario, *Proc. Natl. Acad. Sci. U. S. A.*, 97(18), 9875–9880, 2000.
- Huebert, B. J., T. Bates, P. B. Russell, G. Shi, Y. J. Kim, K. Kawamura, G. Carmichael, and T. Nakajima, An overview of ACE-Asia: Strategies for quantifying the relationships between Asian aerosols and their climatic impacts, *J. Geophys. Res.*, 108(D23), 8633, doi:10.1029/2003JD003550, in press, 2003.
- Intergovernmental Panel on Climate Change (IPCC), *Third Assessment Report, Climate Change 2001: The Scientific Basis*, Cambridge Univ. Press, New York, 2001.
- Jacobson, M. Z., Control of fossil-fuel particulate black carbon and organic matter, possibly the most effective method of slowing global warming, *J. Geophys. Res.*, 107(D19), 4410, doi:10.1029/2001JD001376, 2002.
- Japar, S. M., W. W. Brachaczek, R. A. Gorse, J. M. Norbeck, and W. R. Pierson, The contribution of elemental carbon to the optical properties of rural atmospheric aerosols, *Atmos. Environ.*, 20, 1281–1289, 1986.
- Kalashnikova, O. V., and I. N. Sokolik, Importance of shapes and compositions of wind-blown dust particles for remote sensing at solar wavelengths, *Geophys. Res. Lett.*, 29(10), 1398, doi:10.1029/2002GL014947, 2002.

- Kaufman, Y. J., D. Tanre, O. Dubovik, A. Karnieli, and L. A. Remer, Absorption of sunlight by dust as inferred from satellite and ground-based remote sensing, *Geophys. Res. Lett.*, 28(8), 1479–1482, 2001.
- Liousse, C., H. Cachier, and S. G. Jennings, Optical and thermal measurements of black carbon aerosol content in different environments: Variation of the specific attenuation cross-section, sigma (σ), *Atmos. Environ.*, 27, 1203–1211, 1993.
- Martin, J. H., and S. E. Fitzwater, Iron-deficiency limits phytoplankton growth in the northeast Pacific subarctic, *Nature*, 331(6154), 341–343, 1988.
- Martins, J. V., P. Artaxo, C. Liousse, J. S. Reid, P. V. Hobbs, and Y. J. Kaufman, Effects of black carbon content, particle size, and mixing on light absorption by aerosols from biomass burning in Brazil, *J. Geophys. Res.*, 103(D24), 32,041–32,050, 1998.
- McMurry, P. H., X. Wang, K. Park, and K. Ehara, The relationship between mass and mobility for atmospheric particles: A new technique for measuring particle density, *Aerosol Sci. Technol.*, 36(2), 227–238, 2002.
- Parungo, F., C. Nagamoto, M. Y. Zhou, A. D. A. Hansen, and J. Harris, Aeolian transport of aerosol black carbon from China to the ocean, *Atmos. Environ.*, 28, 3251–3260, 1994.
- Petzold, A., C. Kopp, and R. Niessner, The dependence of the specific attenuation cross-section on black carbon mass fraction and particle size, *Atmos. Environ.*, 31, 661–672, 1997.
- Purcell, E. M., and C. R. Pennypacker, Scattering and absorption of light by non-spherical dielectric grains, *Astrophys. J.*, 186, 705–714, 1973.
- Schauer, J. J., et al., ACE-Asia intercomparison of a thermal-optical method for the determination of particle-phase organic and elemental carbon, *Environ. Sci. Technol.*, 37(5), 993–1001, 2003.
- Seinfeld, J. H., and S. N. Pandis, *Atmospheric Chemistry and Physics: From Air Pollution to Climate Change*, J. Wiley, Hoboken, N. J., 1998.
- Streets, D. G., S. Gupta, S. T. Waldhoff, M. Q. Wang, T. C. Bond, and Y. Y. Bo, Black carbon emissions in China, *Atmos. Environ.*, 35, 4281–4296, 2001.
-
- M. S. Bae, R. M. Duvall, and J. J. Schauer, Environmental Chemistry and Technology Program, University of Wisconsin-Madison, 660 N. Park Street, Madison, WI 53706-1481, USA. (minsbae@hotmail.com; rmduvall@students.wisc.edu; jschauer@enr.wisc.edu)
- P. Y. Chuang, Department of Earth Sciences, University of California, Santa Cruz, 1156 High Street, Santa Cruz, CA 95064, USA. (pchuang@es.ucsc.edu)
- A. Jefferson, Climate Monitoring and Diagnostics Laboratory, NOAA, 325 Broadway, Boulder, CO 80303, USA. (ajefferson@cmdl.noaa.gov)
- J. Kim, Meteorological Research Institute, Korean Meteorological Administration, Seoul 156-720, Republic of Korea. (jykim@metri.re.kr)
- H. Yang and J. Z. Yu, Department of Chemistry, Hong Kong University of Science and Technology, Clear Water Bay, Kowloon, Hong Kong. (chyang@ust.hk; chjianyu@ust.hk)